PROCEEDINGS OF SPIE

SPIEDigitalLibrary.org/conference-proceedings-of-spie

A CMOS image sensor for soft x-ray astronomy

Konstantin Stefanov, Charles Townsend-Rose, Thomas Buggey, James Ivory, Oliver Hetherington, et al.

Konstantin D. Stefanov, Charles Townsend-Rose, Thomas W. Buggey, James Ivory, Oliver Hetherington, Andrew D. Holland, Julian Heymes, Jérôme Pratlong, Georgios Tsiolis, David Morris, Kyriaki Minoglou, Thibaut Prod'homme, Matthew Soman, "A CMOS image sensor for soft x-ray astronomy," Proc. SPIE 12191, X-Ray, Optical, and Infrared Detectors for Astronomy X, 121910N (29 August 2022); doi: 10.1117/12.2630733

SPIE.

Event: SPIE Astronomical Telescopes + Instrumentation, 2022, Montréal, Québec, Canada

A CMOS image sensor for soft X-ray astronomy

Konstantin D. Stefanov*[a], Charles Townsend-Rose[a], Thomas W. Buggey[a], James Ivory[a], Oliver Hetherington[a], Andrew D. Holland[a], Julian Heymes**[a], Jérôme Pratlong[b], Georgios Tsiolis[b], David Morris[b], Kyriaki Minoglou[c], Thibaut Prod'homme[c], Matthew Soman[c]
[a]Centre for Electronic Imaging, The Open University, Walton Hall, Milton Keynes MK7 6AA, UK; [b]Teledyne e2v, 106 Waterhouse Lane, Chelmsford CM1 2QU, UK; [c]ESA-ESTEC, P.O. Box 299, 2200 AG Noordwijk, The Netherlands

ABSTRACT

A monolithic CMOS image sensor based on the pinned photodiode (PPD) and optimized for X-ray imaging in the 300 eV to 5 keV energy range is described. Featuring 40 µm square pixels and 40 µm thick, high resistivity epitaxial silicon, the sensor is fully depleted by reverse substrate bias. Backside illumination (BSI) processing has been used to achieve high X-ray QE, and a dedicated pixel design has been developed for low image lag and high conversion gain. The sensor, called CIS221-X, is manufactured in a 180 nm CMOS process and has three different 512×128-pixel arrays on 40 µm pitch, as well as a 2048×512 array of 10 µm pixels. CIS221-X also features per-column 12-bit ADCs, digital readout via four high-speed LVDS outputs, and can be read out at 45 frames per second. CIS221-X achieves readout noise of 2.6 e- RMS and full width at half maximum (FWHM) at the Mn-K_α 5.9 keV characteristic X-ray line of 153 eV at -40 °C. This paper presents the characterization results of the first backside illuminated CIS221-X, including X-ray response and readout noise. The newly developed sensor and the technology underpinning it is intended for diverse applications, including X-ray astronomy, synchrotron, and X-ray free electron laser light sources.

Keywords: X-ray image sensors, pinned photodiode, X-ray astronomy.

1. INTRODUCTION

Monolithic CMOS image sensors (CIS) are being developed or considered for several planned and proposed space telescopes working in the soft X-ray range. The Einstein Probe[1], expected to launch in 2023, will be using CIS based on the pinned photodiode (PPD) in its wide-field X-ray telescope (WXT). The instrument is intended to cover the 0.5 to 4 keV energy range and will have 12 identical detector modules with 12.3×12.3 cm^2 focal planes, served by four sensors each[2]. With a total sensor area greater than 1800 cm^2, WXT will be one of the biggest space instruments based on CMOS technology.

The proposed Transient High Energy Sources and Early Universe Surveyor (THESEUS)[3] includes the Soft X-ray Imager (SXI), which will have two detector modules using lobster eye optics for a 0.5 srad total field of view, covering the 0.5 to 5 keV energy range. The focal plane will contain an array of eight 3-side buttable CIS, each with size of 8×4 cm^2, for a total of 256 cm^2. The sensors are expected to feature 40 µm square pixels based on the PPD and an active thickness of about 40 µm for high quantum efficiency (QE) and background rejection[4]. Monolithic CIS are also considered for the High Definition X-ray Imager (HDXI) instrument aboard the Lynx X-ray observatory[5] and for the HiZ-GUNDAM mission[6].

Traditionally the domain of the Charge Coupled Device (CCD), CIS can offer many advantages in the field of soft X-ray astronomy. Those include increased radiation hardness, higher operating temperatures, fast readout, and greater system integration due to the on-chip signal digitization. Recent advances in CMOS image sensor technology and the wider availability of high performance, large area devices make CIS a strong candidate for future spaced-based X-ray imaging.

*Konstantin.Stefanov@open.ac.uk; phone +44 1908 332116; https://www.open.ac.uk/science/research/cei/

**Now with Paul Scherrer Institut (PSI), Villigen, Switzerland.

X-Ray, Optical, and Infrared Detectors for Astronomy X, edited by Andrew D. Holland, James Beletic
Proc. of SPIE Vol. 12191, 121910N · © 2022 SPIE · 0277-786X · doi: 10.1117/12.2630733

The Centre for Electronic Imaging (CEI), Teledyne e2v and ESA-ESTEC have been working on a project to develop a prototype CIS optimized for the THESEUS's SXI instrument. Following the characterization[7] of the frontside-illuminated (FSI) variants of the prototype sensor CIS221-X, the work described in this paper covers the first characterization results of the backside-illuminated (BSI) devices.

2. SENSOR REQUIREMENTS

The sensor requirements described in this section have been derived for the SXI, but they are also applicable to many other X-ray astronomy missions and terrestrial applications. The need to reconstruct the signal from X-rays with energy as low as 300 eV means that only BSI devices with a much thinner dead layer than the absorption length (0.14 μm at 300 eV) can be used. Similar to the manufacture of UV imagers, very shallow surface passivation in CIS is routinely applied, allowing the useable energy range to extend to such low energies. Full depletion or even over-depletion of the sensitive silicon material is required to minimize diffusion and charge sharing.

A 300 eV X-ray creates only 82 e^- on average, and the charge could be shared between several pixels. The small signals require very low noise in-pixel source follower transistors, and a tight distribution with a reduced number of higher noise outliers. The required mean system noise is taken as < 5 e^- RMS, but reducing it further to 2 e^- RMS could be of considerable interest.

To reduce the impact of charge sharing, pixels in X-ray sensors tend to be larger than in sensors for visible light. Our studies indicate that the optimal pixel size for the SXI is between 30 and 50 μm. Pinned photodiodes with such large size would have severe image lag if no measures to reduce it are taken. One proven method to improve the image lag is by introducing a small electric field within the PPD to speed up the charge transfer[8].

The active sensor thickness is primarily determined by the absorption length of 5 keV X-rays in silicon, which is approximately 18 μm. However, the radiation background should also be considered for the selection of the detector thickness because particles created by the interaction of space radiation with the instrument shielding can produce signals in the energy range of the X-rays of interest. A simulation of the energy deposition by particles created by galactic cosmic rays, shown in Figure 1, indicates that increasing the sensor thickness moves a large part of the background signal towards higher energies. For a silicon thickness above 35 μm much of the background energy deposition becomes higher than 5 keV, therefore this thickness has been selected for our work.

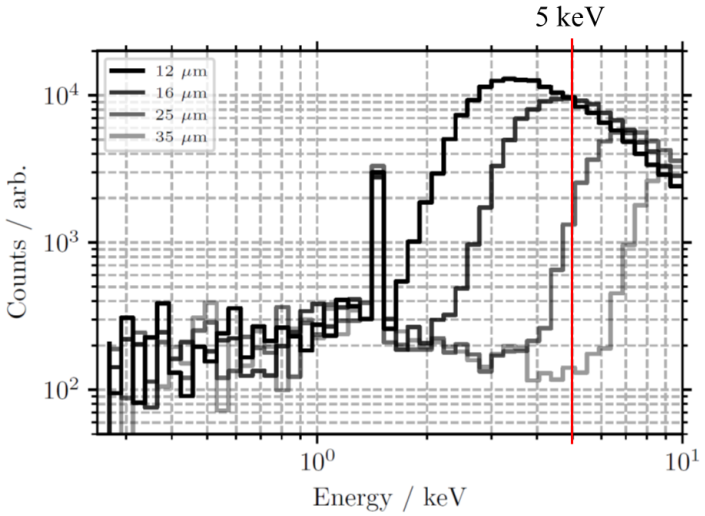

Figure 1. A simulated spectrum of the total deposited energy from galactic cosmic rays in silicon with thickness in the range between 12 μm and 35 μm. A 5 cm thick aluminum shield has been assumed. Figure courtesy of Jonathan Keelan, The Open University.

PPD-based CIS tend to be more radiation hard than CCDs because there is only one charge transfer in the pixel. CCDs suffer from charge transfer inefficiency (CTI) due to radiation-induced bulk traps, and the signal can be severely reduced after several thousand transfers. Normally, CCDs must operate at temperatures as low as -120 °C to mitigate against bulk

traps, by ensuring they stay filled with electrons for a long time. CIS do not have to do that, and the operating temperature is determined primarily by the allowed dark signal and the readout rate. The available power for the SXI allows cooling only to -40 °C, but this temperature should be low enough to accommodate the increase of the dark current due to ionizing and bulk damage[4]. The increased operating temperature reduces the challenges in the design of the SXI instrument.

The typical row-by-row pixel access, and column parallel CIS architecture allows readout rates at tens or hundreds of frames per second (fps). High frame rates are desirable to reduce event pile-up and the signal contribution from dark current, and also for observing fast transient phenomena. On-chip signal digitization using an ADC per column is key to achieving fast readout with low power dissipation and is widely implemented in many scientific CIS. A readout rate higher than 10 fps is envisaged for the SXI, which assumes 12-bit on-chip digitization.

Large area, 3- or 4-side buttable sensors are required for the building of large focal planes. Sensors with size above approximately 2×2 cm^2 are made by reticle stitching and are within the capabilities of many semiconductor foundries. Balancing sensor size and device yield, CIS with size 6×6 cm^2 have been reliably manufactured[9].

Optical blocking filters (OBF) are normally required for X-ray sensors to reduce their responsivity to stray light. An on-chip OBF, usually formed by metal deposition, can be very robust because it uses the sensor's surface for mechanical support, and is the preferred implementation for space applications.

3. DESIGN OF CIS221-X

CIS221-X is based on Teledyne e2v's CIS120 Capella readout architecture[10], and on a subsequent variant with reverse substrate bias. CIS221-X borrows the design of all the peripheral electronics from CIS120, but the image array includes new 40 µm and 10 µm pixels, all designed and simulated in TCAD at the CEI. The block diagram of CIS221-X is shown in Figure 2. The device is manufactured in a 180 nm CMOS image sensor process and has three different 512×128-pixel arrays on 40 µm pitch, as well as a 2048×512 array of 10 µm pixels for benchmarking.

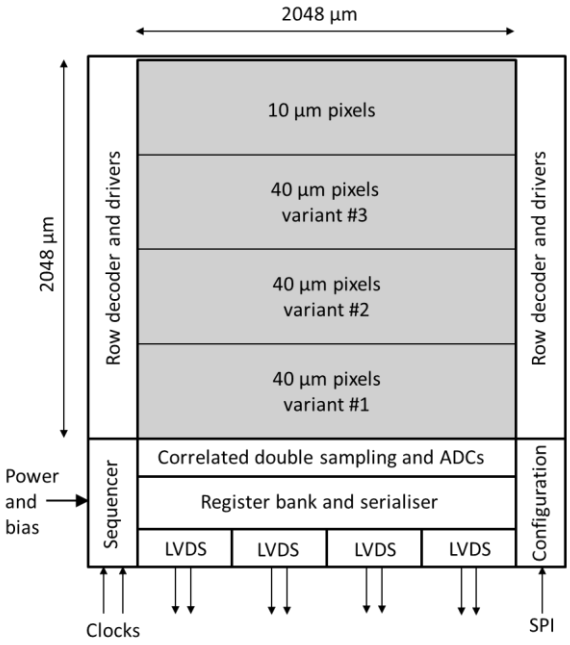

Figure 2. Block diagram of CIS221-X.

The sensor features per-column correlated double sampling and single slope ADCs with programmable resolution. For the expected X-ray signals 12-bit ADC resolution is normally used, although 8-, 10- and 14-bit are also available. The sensor is read out in rolling shutter mode with pixel timing controlled by the sequencer and the frequency of the input clock. The output data are carried by four high speed LVDS outputs and synchronization signals. Most of the functionality, such as the bias currents, ADC resolution, gain and offsets are controlled by configuration registers via serial programming

interface (SPI). The silicon die has all the contacts on the readout side and is 3-side buttable to enable larger focal planes to be built.

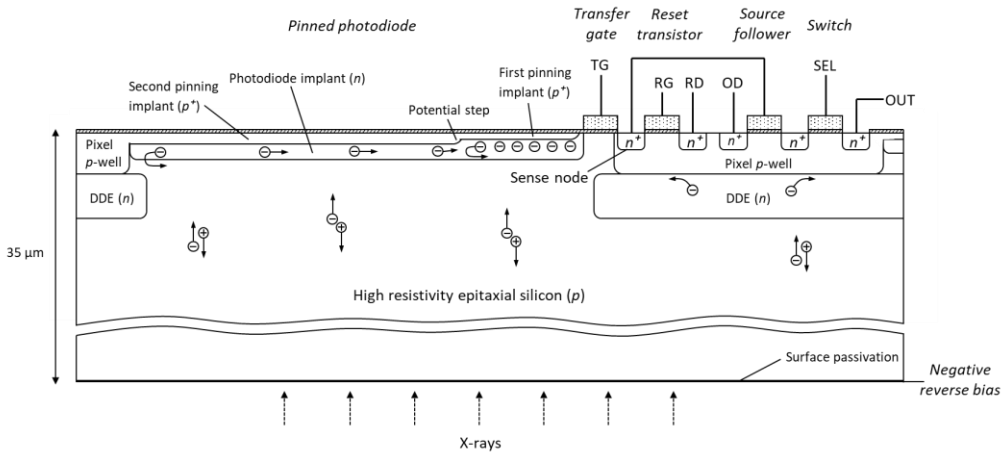

Figure 3. Simplified cross section of the 40 µm pixel in CIS221-X (not to scale).

The total image area is 2.048×2.048 cm^2, evenly distributed between the four pixel types. The pixels use PPDs and can be reverse biased with the help of a deep depletion extension (DDE) implant[11] as shown in Figure 3. To help reduce image lag, the 40 µm PPDs have a second pinning implant over most of the pixel area. As a result, small signal charges are stored close to the transfer gate (TG), where the potential is slightly higher than in the area taken by the second pinning implant. The 40 µm pixel variants have different shapes of this additional implant.

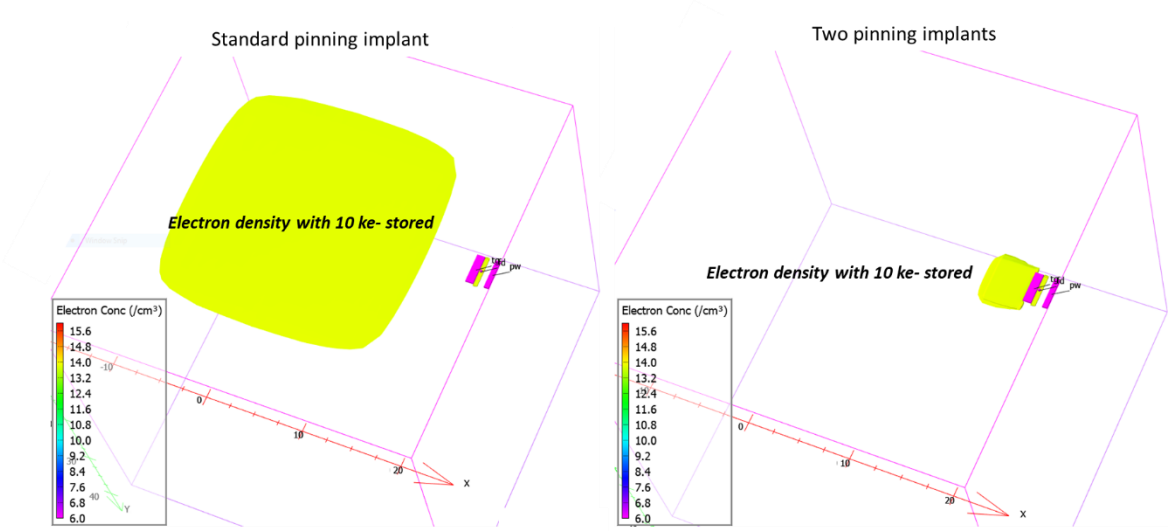

Figure 4. TCAD pixel models with standard and two pinning implants, both containing 10 ke$^-$.

The TCAD models in Figure 4 compare the charge storage volumes between the standard structure and our design in Figure 3. Simulations show that the charge transfer is quick and comparable to much smaller PPDs, and that without these measures the image lag would be too high[4]. Once the charge fills the volume next to the TG it will overflow into the rest of the PPD, from where the charge transfer becomes significantly slower. Since the expected soft X-ray signals contain only a few thousand electrons, the proposed design should work well.

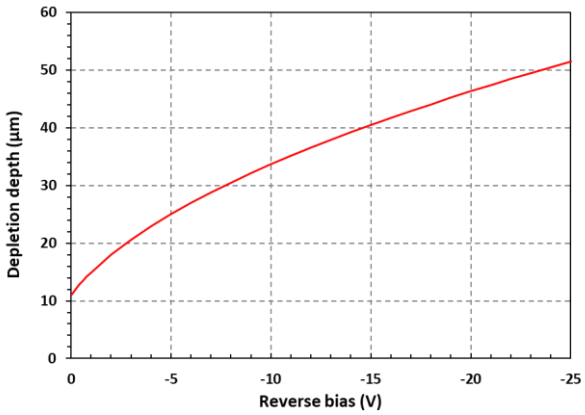

Figure 5. Calculated depletion depth under a pinned photodiode in 1000 Ω.cm *p*-type silicon as a function of the applied reverse bias.

The sensor is built on 40 µm thick, *p*-type epitaxial wafers with typical resistivity of 1000 Ω.cm. Both FSI and BSI devices were fabricated. In the BSI variant, which is of primary interest, the active thickness becomes around 35 µm after wafer thinning and removal of the substrate out-diffusion. Full depletion is expected at -11 V reverse substrate bias, as the calculation in Figure 5 shows. The DDE has been designed to sustain higher reverse voltage with the purpose to allow over-depletion of the epitaxial layer, which helps with reducing charge sharing.

4. CHARACTERISAZION OF THE FIRST BSI DEVICES

4.1 Device variants and packaging

The test setup and the characterization results of the FSI devices have been described previously[7]. The CIS221-X wafers were made in two process splits with different DDE implants. Following the characterization of the FSI imagers, only devices with "medium" DDE implant progressed to BSI processing. The BSI CIS221-X have ceramic pin grid array (PGA) package, shown in Figure 6, which is more robust and easier to handle than the package of the FSI variant. The first batch of BSI devices was received in June 2022 and the following sections present initial characterization results.

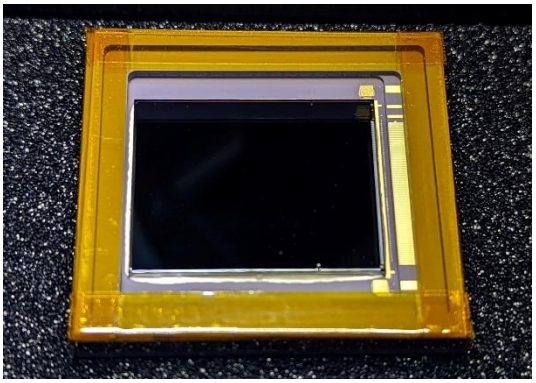

Figure 6. Backside illuminated CIS221-X in a ceramic PGA package.

4.2 Reverse leakage current

The substrate I-V characteristic under reverse bias is used to determine the voltage at which the leakage current becomes significant and is an important indicator of the maximum possible reverse voltage and the depletion conditions. Figure 7 shows the I-V characteristic of one device, taken while the sensor is performing normal imaging with all clocks and biases applied. At -40 °C the onset of higher leakage is around -20 V, indicating that over-depletion can be achieved. Most of the subsequent characterization is carried out at a reverse backside bias V_{BSB} of -20 V.

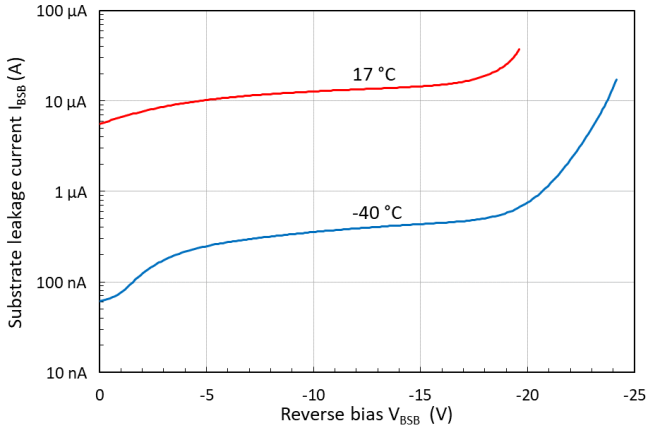

Figure 7. Reverse leakage current for the whole sensor (Serial #21094-03-11) during normal operation at 17 °C and -40 °C.

The leakage current includes the image array and all the peripheral CMOS circuits, and at around 1 µA is acceptable for a device with a total image area of 4.2 cm^2. The contribution of the dark current in the whole image array is around 100 pA, measured from images taken at increasing integration times. The leakage current in the pixel array above approximately -20 V (at -40 °C in Figure 7) is composed of holes[11], therefore the leakage charge does not accumulate in the potential wells in the PPDs and there is no noticeable effect on the device's performance even at reverse currents reaching tens of microamps.

4.3 Readout noise and frame rate

The readout noise was measured in darkness and without clocking the transfer gate, so that the dark signal integrated in the PPD is not transferred to the sense node. The RMS pixel noise, derived from the histogram in Figure 8(a) is 2.6 e^-. The cumulative noise distribution in Figure 8(b) shows that 90% of the pixels have noise below 2.8 e^- RMS.

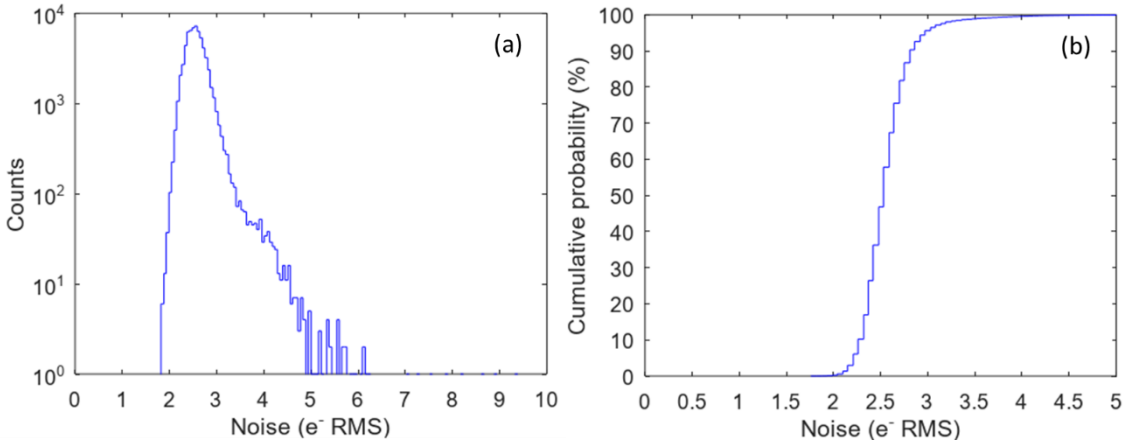

Figure 8. Pixel noise distribution (a) and the corresponding cumulative noise (b) at -40 °C.

One of the reasons for the good noise performance is that special attention has been paid to minimizing the sense node capacitance. This increases the conversion gain, estimated at 70 µV/e^-, and reduces the input-referred noise of the in-pixel source follower. Even better noise performance appears possible in this CMOS image sensor process. The source follower noise in transistors using the same geometry as in CIS221-X, but in a separate device using analog readout has been measured at 1.8 e^- RMS.

The CIS120 architecture is rated of 20 fps, reading 2048×2048 pixels at 12-bit resolution. When reading the whole image area including the 10 µm and 40 µm pixels, CIS221-X dissipates about 400 mW and is capable of 45 fps. An imager of the same physical size containing only 40 µm pixels would be able to achieve 320 fps using a slightly modified readout architecture.

4.4 X-ray response

Only the 40 µm pixel variant #3 has been presented here because during the previous FSI characterization it was established that its image lag was much better than the other two variants. The BSI CIS221-X was illuminated with fluorescence X-rays from a manganese target, excited by an X-ray tube. The unprocessed X-ray spectrum is shown in Figure 9. It shows several other fluorescence lines from the walls of the vacuum vessel (Fe, Ni and Cr) and the aluminum support of the target.

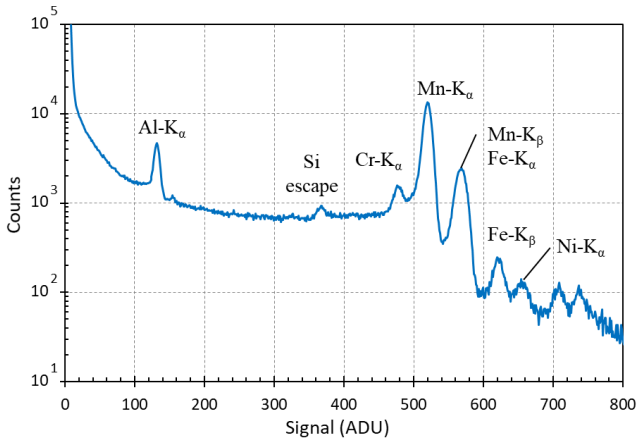

Figure 9. X-ray fluorescence spectrum from a manganese target obtained with the 40 µm pixel variant #3 at -40 °C and V_{BSB} = -20 V.

The charge deposited only in a single pixel is found by requiring that the central pixel in a 3×3-pixel area contains >95% of the total charge from the sum of all signals. A histogram of the single pixel X-ray events using this method is shown in Figure 10.

The energy resolution at the Mn-K_α 5.9 keV line is often used as a benchmark for the performance of a sensor. In the data in Figure 10, the full width at half maximum (FWHM) of the Mn-K_α peak is 153±5 eV. This is higher that the previously reported resolution of 142 eV in an FSI device with different DDE implant[7], however we believe that there is further room for improvement by optimization of the operating conditions and performing per-pixel gain calibration.

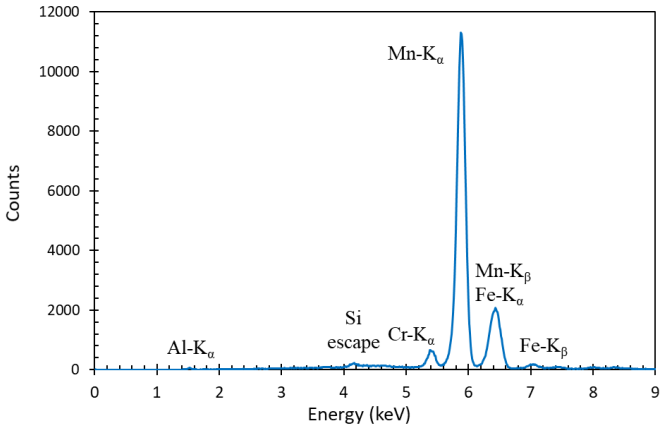

Figure 10. Single pixel events from the spectrum in Figure 8 using the energy calibration from the Mn-K_α line.

5. CONCLUSIONS AND FUTURE WORK

The first BSI CIS221-X devices work well and show very good performance as soft X-ray imagers. This has been made possible by a custom design using 40 µm pixels with low image lag, full depletion of the 35 µm thick epitaxial layer and

high conversion gain for low readout noise. The measured FWHM at the Mn-K_α peak is 153 eV and the readout noise is 2.6 e^- RMS. We are presently investigating the dark current dependence on the temperature and the effect of the reverse bias on the charge sharing of X-ray signals. We are also expecting to receive a device batch with an OBF applied to one half of the image area, which should allow us to evaluate the effectiveness and the quality of the coating. Further work will include radiation damage characterization using gamma, proton and heavy ion irradiations, and QE measurements in the X-ray range of interest.

ACKNOWLEDGEMENTS

This work is funded by ESA under the E/0901-01 Technology Development Element "CMOS Image Sensor for X-ray Applications", contract No. 4000129545/19/NL/AR.

REFERENCES

[1] Yuan, W. et al., "Einstein Probe: a lobster-eye telescope for monitoring the x-ray sky". Proc. SPIE 1069925 (2018), doi:10.1117/12.2313358.
[2] Wang, W. et al., "Developments of scientific CMOS as focal plane detector for Einstein Probe mission", Proc. SPIE 106995O (2018), doi:10.1117/12.2311922.
[3] Amati, L. et al., "The THESEUS space mission: updated design, profile and expected performances", Proc. SPIE 114442J (2021), doi:10.1117/12.2561297.
[4] Heymes, J. et al., "Development of a photon-counting near-Fano-limited X-ray CMOS Image Sensor for THESEUS' SXI", Proc. SPIE 114540I (2020), doi: 10.1117/12.2560162.
[5] Falcone, A. D. et al., "Overview of the high-definition x-ray imager instrument on the Lynx x-ray surveyor", J. Astron. Telesc. Instrum. Syst., 5(2), 021019 (2019), doi:10.1117/1.JATIS.5.2.021019.
[6] Ogino, N. et al., "Performance verification of next-generation Si CMOS soft X-ray detector for space applications", Nucl. Instr. Meth. Phys. Research, A987, 164843 (2021). doi:10.1016/j.nima.2020.164843.
[7] Heymes, J. et al., "Characterisation of a soft X-ray optimised CMOS Image Sensor", Journal of Instrumentation, 17, P05003 (2022), doi:10.1088/1748-0221/17/05/P05003.
[8] Miyauchi, K. et al. "Pixel structure with 10 nsec fully charge transfer time for the 20m frame per second burst CMOS image sensor", Proc. SPIE 902203 (2014), doi: 10.1117/12.2042373
[9] Wu, Q. et al., "X-Ray Performance of a Customized Large-format Scientific CMOS Detector", Publications of the Astronomical Society of the Pacific, 134(1033), 035006 (2022), doi:10.1088/1538-3873/ac5ac9.
[10] Jorden, P.R. et al., "Teledyne e2v sensors optimised for ground-based and space applications", Proc. SPIE 1070903 (2018), doi:10.1117/12.2310097.
[11] Stefanov, K.D., Clarke, A.S., Ivory, J. and Holland, A.D., "Design and Performance of a Pinned Photodiode CMOS Image Sensor Using Reverse Substrate Bias," Sensors 18, 118 (2018), doi:10.3390/s18010118.